Convective pattern on the surface of the giant star π^1 Gruis

C. Paladini[1,2], F. Baron[3], A. Jorissen[1], J.-B. Le Bouquin[4], B. Freytag[5], S. Van Eck[1], M. Wittkowski[6], J. Hron[7], A. Chiavassa[8], J.-P. Berger[3,5], C. Siopis[1], A. Mayer[6], G. Sadowski[1], K. Kravchenko[1], S. Shetye[1], F. Kerschbaum[6], J. Kluska[9], S. Ramstedt[5]

[1]*Institut d'Astronomie et d'Astrophysique, Université libre de Bruxelles, CP 226, 1050 Bruxelles, Belgium*
[2]*European Southern Observatory, Alonso de Cordova 3107, Vitacura, Santiago, Chile*
[3]*Department of Physics and Astronomy, Georgia State University, P.O. Box 5060 Atlanta, GA30302-5060, USA*
[4]*Université Grenoble Alpes, CNRS, IPAG, 38000 Grenoble, France*
[5] *Department of Physics and Astronomy, Uppsala University, Box 516, 75120 Uppsala, Sweden*
[6] *European Southern Observatory, Karl-Schwarzschild-Strasse 2, 85748 Garching bei München, Germany*
[7] *Department of Astrophysics, University of Vienna, Türkenschanzstrasse 17, 1180 Vienna, Austria*
[8] *Laboratoire Lagrange, UMR 7293, Université de Nice Sophia-Antipolis, CNRS, Observatoire de la Côte d'Azur, BP. 4229, 06304 Nice Cedex 4, France*
[9] *University of Exeter, Department of Physics and Astronomy, Stocker Road, Exeter, Devon EX44QL, UK*

Convection plays a major role for many types of astrophysical processes[1,2] including energy transport, pulsation, dynamo, wind of evolved stars, dust clouds on brown dwarfs. So far most of our knowledge about stellar convection has come from the Sun. Of the order of two million convective cells of typical size ~2000 kilometers are present on the Solar surface[3], a phenomenon known as granulation. But on the surface of giant and supergiant stars, which can be few hundred times larger than the Sun, the low surface gravities should engender only a few large convective cells[3]. Deriving characteristic properties of convection (like granule size and contrast) for the most evolved giant and supergiant objects is a difficult task. In those stars, the photosphere is obscured by dust, which partially masks the convective patterns, making their measurement difficult[4]. But when the photosphere was accessible to observations, the properties of convection were so far inferred from model-dependent fitting of asymmetric structures[5,6,7]. This indirect method provides however no clue about the physical origin of the fitted spots[5,6,7]. Here we present interferometric images of the surface of the evolved giant star π^1 Gruis, of spectral type S5,7[8,9] denoting a star with strong ZrO bands in its spectrum. Our images show a nearly circular dust-free atmosphere, which is very compact and weakly affected by molecular opacities. We find that the stellar surface shows a complex convective pattern with an average intensity contrast of 12% that increases towards shorter wavelengths. Through the analysis of the power spectrum of the images we derive a characteristic horizontal granulation size of $(1.2 \pm 0.2) \times 10^{11}$ m, corresponding to 27% of the stellar diameter. Our measurements fall along the scaling relations between convective cell size, effective temperature, and surface gravity predicted by the mixing-length theory and multi-dimensional radiation-hydrodynamic simulations of stellar surface convection[10,11,12].

π^1 Gruis was observed with the 4-telescope H-band beam combiner PIONIER[13] mounted at the Very Large Telescope Interferometer (Cerro Paranal, Chile) during the nights of 2014 September 25 and 29. The observations (see also the Data section in Methods) cover three spectral channels across the near-infrared H-band (central wavelengths are 1.625, 1.678, and 1.730 µm; the width of the filters is 0.0483 µm, corresponding to a spectral resolution of 35). Thanks to the excellent Fourier plane coverage acquired, and to the good signal-to-noise ratio (Extended data Fig. 1), we are able to reconstruct model-independent images in each spectral channel (Fig. 1). For this purpose, we use the image reconstruction software SQUEEZE[14], based on a Markov chain Monte Carlo (MCMC) approach to the regularized maximum likelihood problem. To assess the reliability of the image we also use a different image reconstruction algorithm, MiRa[15]. The images from SQUEEZE and MiRa have very similar characteristics and are shown in Fig. 1 (see also the Image Reconstruction section in Methods). The dusty envelope enshrouding the star is transparent in the wavelength range of our observations. The major molecular contributions in this wavelength range are CO and CN; this molecular contribution is the weakest in the longest-wavelength filter, which can be considered as probing the continuum. The images show a stellar disc with the diameter weakly dependent on the wavelength, thus pointing to the fact that the molecular envelope is very shallow, and we are probing the stellar surface. There are patchy structures all well within the nearly circular stellar surface (as opposed for instance to the situation of the well studied[7,16] supergiant Betelgeuse). For all these reasons, we may infer that the patterns seen on the stellar surface are the actual convective granules. Arguably this is the most detailed model-independent (see the Image Reconstruction section in Methods) image of convective patterns on the surface of a giant star ever obtained.

We estimated the intensity contrast[17] $\Delta I_{\mathrm{rms}}/\langle I \rangle$, after correcting the intensity profile I for the limb darkening effect (see the Power Spectrum section in Methods). This correction ensures that the contrast is only sensitive to the convective pattern. We obtain 13.1 ± 0.2%, 12.3 ± 0.4%, and 11.9 ± 0.4% in the three spectral channels (ordered by increasing wavelength), where the (statistical) uncertainty corresponds to the standard deviation of the contrast on the various images produced by the Markov-chain Monte-Carlo approach used within the SQUEEZE code (see the Image Reconstruction section in Methods). The contrast measurements show a trend towards higher values at shorter wavelengths, going along with a stronger molecular contamination. The 3D models[18, 19] of red giants are still at an exploratory stage, and they do not cover the parameter space of π^1 Gru. Such models predict for the surface convective motions a bolometric intensity contrast of the order of 20%, and contrasts in the H-band, as observed here, may be expected to be lower. Systematic errors (coming from seeing, limited resolution...), that are difficult to assess quantitatively, are also expected to make the observed contrast lower. The above effects (and others) were discussed in the context of direct imaging of solar granulation[11,17], but they are likely to reduce the contrast in the interferometric context considered here as well.

The prospect offered by the granule size in that respect is much better. While in previous studies[5,6,7], this quantity was obtained via model fitting, often unconvincingly because of the high values of the resulting reduced χ^2, our interferometric model-independent images allow us for the first time to derive the granule size directly from a spatial power-spectrum density (PSD) analysis. This technique is routinely applied on theoretical model predictions[10,11,12], and is used here to derive the wavenumber ($k = 2\pi\xi$; where $\xi = 1/\lambda$ is the number of wavelengths per unit of distance, not to be confused with the wavelengths of the observations) carrying the maximum power, i.e., the characteristic granule size. The left panel of Figure 2 shows the power spectral density as a function of spatial frequency for the three spectral channels of the PIONIER SQUEEZE image-cube. After smoothing the PSD of the three spectral channels to remove the wiggles of the curve, we derive the maximum of the PSD by averaging the position of the three peaks. The error is calculated as the standard deviation of the latter three values. The resulting granulation size is 5.3±0.5 mas. The PSD from the MiRa images gives very similar results (right panel of Fig.2), and the granulation size agrees within the error with the one derived from the SQUEEZE images. It is not possible to directly compare this observed value with a global model atmosphere matching π^1 Gru since such a model does not exist. Clearly, stellar surface convection does not look the same all across the HR diagram in terms, for instance, of granulation size. However, if stellar convection obeys the same (magneto-)radiation-hydrodynamic processes all across the HR diagram, it may be hoped that the parametric formulae relating the characteristic granule size to the stellar parameters, based on predictions from the mixing-length theory of convection[20] and from models for less-evolved stars[10,11,12], could be applicable to π^1 Gru as well.

In order to perform this comparison between the spatial structure detected at the surface of π^1 Gru and these parametric relations, we convert the typical angular size of the granules observed at the surface of π^1 Gruis into linear size. We use π^1 Gruis parallax of 6.13 ± 0.76 mas[21], yielding a characteristic linear granule size $x_g = (1.2 \pm 0.2) \times 10^{11}$ m. The comparison requires as well the knowledge of π^1 Gruis atmospheric parameters (see the Stellar parameters section in Methods): $T_{\mathrm{eff}} = 3200$ K, $\log g = -0.4$, solar metallicity, and mean molecular weight $\mu = 1.3$ g mole^{-1} for a non-ionized solar mixture with 75% H and 25% He in mass.

The mixing length theory of convection predicts that the characteristic granule size x_g scales linearly with the pressure scale-height H_p[10]:

$$x_g = 10\, H_p$$

where $H_p = T_{\rm eff}\, R_{\rm gas}\, (\mu g)^{-1}$, and where $R_{\rm gas} = 8.314 \times 10^{7}$ erg K^{-1} mole^{-1} is the gas constant. The proportionality factor of 10 ensures that the formula correctly predicts the granulation at the surface of the Sun (Ref. 11 and Fig. 3). Expressing x_g in units of 10^6 m, g in cgs, and $T_{\rm eff}$ in Kelvin, Eq. (1) becomes[10]:

$$\log x_g = \log T_{\rm eff} - \log g - \log \mu + 0.92 \ (2)$$

or $x_g = 5.1 \times 10^{10}$ m with π^1 Gruis atmospheric parameters. More recent 3D models[12] have extended this early analysis to FGK dwarfs and K giants, and predict the size of the convective granules to depend on the stellar parameters in a way very similar to the above relation (with the same units as above):

$$\log x_{g,\ \rm Trampedach} = (1.321 \pm 0.004)\, T_{\rm eff} - (1.0970 \pm 0.0003) \log g + (0.031 \pm 0.036)$$

This relation yields $x_{g,\rm Trampedach} = 1.2 \times 10^{11}$ m for π^1 Gruis. Finally, the CIFIST grid[11,22] covers also M-type stars, and sub-solar metallicities (expressed as $[{\rm Fe/H}] = \log_{10}\left({\rm N(Fe)}/{\rm N}(H)\right)_{\rm star} - \log_{10}\left({\rm N(Fe)}/{\rm N}(H)\right)_{\odot}$, where N(A) is the number density of element A and $\odot$ denotes the Sun). It follows[11]:

$$\log x_{g,\ \rm Tremblay} = 1.75\ \log({\rm T_{eff}} - 300\ \log g) - \log g + 0.05[{\rm Fe/H}] - 1.87$$

i.e., $x_{g,\rm Tremblay} = 4.9 \times 10^{10}$ m for π^1 Gruis. Despite the fact that none of the above relations rely on stellar models matching π^1 Gruis atmospheric parameters (corresponding to a very evolved late-type giant star), their predictions are in fairly good agreement as it is shown in Fig. 3. This result suggests that predictions from current models of stellar surface convection may be extrapolated in a fairly satisfactory way to the region of the Hertzsprung-Russell diagram where luminous red giants are located. Finally, in the future, studies such as this should secure time-series images to address the issue of the lifetime of the observed convective structures, which is another important way of comparing observations with model predictions.

1. Gimenez A., *et al.*, Theory and Tests of convection in Stellar Structure, *ASP Conference Series* **173**, 391 pp. (1999).
2. Kupka F., Convection in Stars, The A star Puzzle, eds. J. Zverko et al., *Cambridge Univ. Press, IAU Symp.* **224**, 119-129, (2004).
3. Schwarzschild M., On the scale of photospheric convection in red giants and supergiants, *Astrophys. J.* **195**, 137 – 144 (1975).
4. Wittkowski M., *et al.*, Aperture synthesis imaging of the carbon AGB star R Sculptoris: Detection of a complex structure and a dominating spot on the stellar disk, *Astron. Astrophys.* **601**, 3 (2017).
5. Young J. S., *et al.*, New views of Betelgeuse: multi-wavelength surface imaging and implications for models of hotspot generation, *Mon. Not. R. Astron. Soc.* **315**, 635 – 645 (2000).
6. Haubois X., Perrin G., Lacour S., Imaging the spotty surface of Betelgeuse in the H band, *Astron. Astrophys.* **508**, 923 (2009).
7. Montarges M., *et al.*, The close circumstellar environment of Betelgeuse. IV. VLTI-PIONIER interferometric monitoring of the photosphere, *Astron. Astrophys.* **588**, A130 (2016).
8. Keenan P. C., Classification of the S-Type Stars, *Astroph. J.* **120**, 484-505 (1954)
9. Mayer A., *et al.*, Large-scale environments of binary AGB stars probed by Herschel. II. Two companions interacting with the wind of π^1 Gruis, *Astron. Astrophys.* **570**, A113 (2014).
10. Freytag B., Holweger H., Steffen M., Ludwig H.-G., On the Scale of Photospheric Convection, in: Science with the VLT Interferometer (Proceedings of the ESO workshop), Springer (Berlin, New York), 316-317 (1997).
11. Tremblay P.-E., *et al.*, Granulation properties of giants, dwarfs, and white dwarfs from the CIFIST 3D model atmosphere grid, *Astron. Astrophys.* **557**, A7 (2013).
12. Trampedach R., *et al.*, A Grid of Three-dimensional Stellar Atmosphere Models of Solar Metallicity. I. General Properties, Granulation, and Atmospheric Expansion, *Astrophys. J.* **769,** A18 (2013).
13. Le Bouquin, J.-B., *et al.*, PIONIER: a 4-telescope visitor instrument at VLTI, *Astron. Astrophys.* **535**, A67 (2011).
14. Baron F., Monnier J. D., Kloppenborg B., A novel image reconstruction software for optical/infrared interferometry, *Proc. SPIE* **7734**, 77342I (2010).

15. Thiébaut, É., MiRA: an effective imaging algorithm for optical interferometry, *Proc. SPIE* **7013**, 70131I (2008).
16. Kervella P., *et al.*, The close circumstellar environment of Betelgeuse. II. Diffraction-limited spectro-imaging from 7.76 to 19.50 µm with VLT/VISIR, *Astron. Astrophys.* **531**, A117 (2011).
17. Wedemeyer-Böhm S., Rouppe van der Voort L., On the continuum intensity distribution of the solar photosphere, *Astron. Astrophys.* **503**, 225-239 (2009).
18. Freytag B., Höfner S., Three-dimensional simulations of the atmosphere of an AGB star, *Astron. Astrophys.* **483**, 571-583 (2008).
19. Freytag B., Liljegren S., Höfner S., Global 3D radiation-hydrodynamics models of AGB stars. Effects of convection and radial pulsations on atmospheric structures, *Astron. Astrophys.* **600**, A137 (2017).
20. Ulrich R. K., Convective Energy Transport in Stellar Atmospheres. I: A Convective Thermal Model, *Ap&SS* **7**, 71-86 (1970).
21. van Leeuwen F., Validation of the new Hipparcos reduction, *Astron. Astrophys.* **474**, 653 – 664 (2007).
22. Ludwig H.-G., *et al.*, The CIFIST 3D model atmosphere grid, *Mem. Soc. Astron. It.* **80**, 711-714 (2009).

Full Methods and associated references are available online.

Acknowledgements

C.P. acknowledges the support of the Fonds National de la Recherche Scientifique (F.R.S.-FNRS), Belgium. C.S., G.S. are supported by the PRODEX office, Belgium. This research has been funded by the Belgian Science Policy Office under contract BR/143/A2/STARLAB (S.S., A.J., S.vE.). K.K. is supported by a FRIA grant (Belgium). FB acknowledges funding by the National Science Foundation, NSF-AST numbers 1445935 and 1616483. J.K. acknowledges the Philip Leverhulme Prize (PLP-2013-110). The research leading to these results has received funding from the European Union's Horizon 2020 research and innovation programme under Grant Agreement 730890 (OPTICON).
We thank all the ESO/VLTI staff for supporting our observations.

Author Contributions

This project was initiated by C.P.. A.M. carried out the observations. J.B.LB. performed the data reduction, F.B. and J.B.LB. performed the image reconstruction. The contrast and the power spectrum analysis was carried on by C.P., B.F. and F.B.. The stellar parameter determination was made by C.P., S.V.E., S.S., and K.K.. A.J. gave crucial help through all the scientific analysis. The text was written by C.P., F.B. and A.J., and edited by the other authors that contributed to the scientific discussion.

Author Information

Reprints and permissions information is available at www.nature.com/reprints.
The authors declare no competing financial interests. Correspondence and requests for material should be addressed to C. P. (cpaladin@eso.org).

Figure 1: The stellar surface of π^1 Gruis. Image of the stellar surface of π^1 Gruis reconstructed from the interferometric data using the SQUEEZE[14] algorithm (upper panels), or the MiRa[15] algorithm (lower panels). From left to right are images in the spectral channels centered on 1.625 µm (a, a'), 1.678 µm (b, b') and 1.730 µm (c, c'). The angular resolution of the observations is $\lambda/2\mathrm{B} \sim 2$ mas and is represented with a circle at the bottom right of panel a). In the images one pixel corresponds to 0.45 mas.

Figure 2: Power spectral density. Left panel: the resulting power spectrum from the SQUEEZE images in three different PIONIER spectral channels. The granulation size is derived by averaging the maximum of the three curves after smoothing.
Right panel: comparison between the power spectrum of the SQUEEZE and MiRa images corresponding to the first spectral channel of PIONIER (1.625 µm). The peak of the MiRa images corresponds to a granulation size consistent (within the error bar) with the one derived from the SQUEEZE image. The grey shaded area on the left marks the limit of the box of the image, the grey shaded area on the right marks the limit of the angular resolution of our observations ($\lambda/2\mathrm{B}$, as indicated on Fig. 1).

Figure 3: The characteristic horizontal scale of granulation of π^1 Gru versus theoretical predictions. The characteristic granulation size obtained from the PIONIER images of π^1 Gru (triangle) is quite different from the solar value (circle). Despite the fact that theoretical predictions (dashed line[10], dotted line[11], and thick line[12]), had to be extrapolated to match π^1 Gru stellar parameters (T_{eff} = 3200 K, log g = −0.44), they are in good agreement with the observations.

Methods

Data

The target of this study was observed with the PIONIER[13] instrument mounted at the Very Large Telescope Interferometer (VLTI, Cerro Paranal). The light from the four Auxiliary Telescopes (ATs), with 1.8 m aperture, was combined to obtain 303 spectrally-dispersed visibilities and 201 closure phases (Extended data Fig.1). The maximum baseline used to collect the observations is 90 m corresponding to an array angular resolution λ/2B (where B stands for baseline, the distance between two apertures) of approximately 2 mas. The data reduction was performed using the `pndrs` package[13]. Following the standard procedure of PIONIER data reduction, the calibrated data are the average of 5 consecutive files of each observing block. A systematic relative uncertainty of 5% is added on the data. The stars HD 209688 (with a diameter[23] 2.62 ± 0.03 mas) and HD 215104 (with diameter[24] 1.7 ± 0.1 mas) were used as calibrators. These objects were selected by using the SearchCal tool developed by the Jean-Marie Mariotti Center (JMMC).

Image Reconstruction

The image reconstruction was performed using two different algorithms, SQUEEZE[14] and MiRA[15], to assess the reliability of the image reconstruction process. Using regularized maximum likelihood, MiRA minimizes a joint criterion which is the sum of (1) a likelihood term which measures the compatibility with the data, and (2) a regularization term which imposes priors on the image. The relative weight between these two terms is controlled by the "hyperparameter" factor μ, and we use the so-called L-curve approach to estimate its optimal value for each regularizer[25]. The output image is 64×64 - pixel wide, with a pixel scale of 0.45 mas pixel^{-1}. After testing different priors and regularizations to identify possible spurious structures in the reconstructions, we concluded that a trustworthy image is obtained with the MiRA smoothness regularizer, without a prior image. SQUEEZE is based on a Markov-chain Monte Carlo (MCMC) approach to the regularized maximum-likelihood problem. It implements parallel simulated annealing and parallel tempering methods, enabling the use of non-convex or non-smooth regularizations that are not implemented in MiRA. SQUEEZE can also handle multi-wavelength data sets with again possibly non-convex and non-smooth trans-spectral regularizations. The π^1 Gruis images were reconstructed with the same pixel scale and field of view as used for the MiRA reconstruction.

We first ran fifty independent, parallel, simulated annealing MCMC chains of 16x16-pixel reconstructions at a quarter of the final resolution (1.8 mas/pixel). Then we ran fifty MCMC chains of 32x32-pixel images at half the final resolution (0.9 mas/pixel), initializing the chains using the mean image over the chains of the 16x16-pixel run. Finally we ran fifty chains of 64x64-pixel reconstruction at full resolution (0.45 mas/pixel), initializing the chains with the mean image of the 32x32-pixel run. The final reconstruction is again the mean image over the 64x64-pixel chains. The whole procedure is designed to avoid falling into local minima, making sure the image is optimal at the lower resolutions before moving on to filling finer details.

Since selecting an adequate regularization is crucial for imaging quality, we determined an adequate combination of regularizers and regularizer weights by simulation. We generated "ground-truth" images of spotless and spotted limb-darkened discs, and using our code OIFITS-SIM we produced OIFITS data with the same (u,v)-coverage and signal-to-noise as the original π^1 Gruis data set. Then we followed the reconstruction procedure described above for several combinations of regularizers known to work for stellar surfaces (entropy, total variation, l_0 pseudo-norm, field-of-view centering, wavelets, …) and regularizer weights. We then selected the "optimal" combination/weights as the one that minimized the absolute mean difference between the reconstructions and the ground-truth discs: i.e. they do not introduce features to the featureless discs, and recover well existing spots. We found that a combination of spot regularizer[26] and l_0 sparsity in the image plane gave the best result.

The final SQUEEZE image has a reduced $\chi^2 \sim 1.3$ and is remarkably similar to the image reconstructed with MiRA. Images at one MCMC standard deviation from the mean display the same features overall, though the details of the bright spots do differ slightly (Extended Data Fig. 2). It should be noted that our reconstructions were done on the three PIONIER spectral channels independently. For comparison SQUEEZE was also used in polychromatic mode (using total variation as a transpectral regularizer), but we did not find any major differences between the polychromatic images and the channel-by-channel approach.

Power spectrum

The power spectral density is the integral over rings comprising wavenumbers in a certain interval around $k = 2\pi\xi$*; where* $\xi = 1/\lambda$ *is the number of wavelengths per unit of distance* of the squared amplitude of the 2-dimensional Fourier transform of the image[17]. The power-spectrum analysis of the original images produces a dominant peak at the wavenumber corresponding to the diameter of the star, followed by several lobes containing information of higher order. To be able to separate the peak associated with the typical granule size from the one associated to the stellar diameter, one needs to subtract first the stellar disc from the image. To perform this step we designed two circular masks (one based on a Gaussian intensity profile, and another on the MARCS model best fitting the photometry), and a square mask fully enclosed on the stellar surface. Both the Gaussian and the MARCS intensity profiles introduce some spurious signal in the final PSD, due to the fact that the intensity profile does not match well the reconstructed one. In particular, the MARCS intensity profile is steeper than the observed one. The square mask provides a final image which is 24x24 pixels, and is free of the limb effects. The square mask is the one providing the cleanest PSD, and it is therefore the one discussed in the paper (Fig.2).

Before proceeding with the PSD analysis, we increased the number of padding points and rescaled the background of the image to the mean intensity of the stellar surface. The method was applied as well to the MiRA image, which delivers a power spectral density very similar to the one derived from the SQUEEZE image, as shown in Fig. 2.

Stellar parameters

The stellar parameters of π^1 Gruis available from the literature[9] are effective temperature of 3100 K, a luminosity[9] of 7200 $L_\odot$, and a current mass[9] of 1.5 $M_\odot$. Taking advantage of the new grid[27] of MARCS models with S-type chemistry, we decided to perform a new parameter estimation. On the basis of the literature values, we calculated a small grid of models covering the following parameter space: $2000 \leq T_{\mathrm{eff}} \leq 3200$ K, with steps of 200 K; log $g = 0$ and -0.44; 1, 1.3, and 2 solar masses; [s/Fe] = 1 and 2 dex; C/O = 0.5, 0.752, 0.899, 0.925, 0.951, 0.971, and 0.991; microturbulence = 2 km s^{-1}. The parameters of the model reproducing best the photometry (Extended data Figure 3), which are later used for the comparison with the theoretical equations of the granule size, are $T_{\mathrm{eff}} = 3200$ K, log g = -0.44, solar metallicity, s-process element abundances enhanced by 1 dex, and C/O = 0.991. These values are in agreement with the literature ones. The diameter of π^1 Gruis was derived by fitting the PIONIER visibility data with a uniform disc. This choice is justified because intensity profiles derived from the MARCS model atmospheres are very similar to a uniform disc in the first visibility lobe. For the fitting we used the LitPro program provided by the JMMC.

The equivalent UD diameter derived is 18.37 ± 0.18 mas, which corresponds to about 658 solar diameter for a parallax[21] of 6.13 mas. Our diameter estimation is in agreement with the literature values[9,28].

Code availability

The image reconstruction code SQUEEZE is publicly available at:
https://github.com/fabienbaron/squeeze
The image reconstruction code MiRa is publicly available at:
https://github.com/emmt/MiRA

Data availability

The reduced PIONIER data sets are available in the http://oidb.jmmc.fr/ repository.

Additional Reference

23. Bordé P., Coudé du Foresto V., Chagnon G., Perrin G., A catalogue of calibrator stars for long baseline stellar interferometry, *Astron. Astrophys.* **393**, 183–193 (2002).
24. Lafrasse S., et al., Building the 'JMMC Stellar Diameters Catalog' using SearchCal, *Proc. SPIE* **7013**, 77344E11 (2010).
25. Renard S., Thiébaut E., Malbet F., Image reconstruction in optical interferometry: benchmarking the regularization, *Astron. Astrophys.* **533**, A64 (2011).
26. Baron F., Monnier J., Young J., Buscher D., New Theoretical Frameworks for Interferometric Imaging, in: Resolving the future of astronomy with long-baseline interferometry, edited by Michelle J. Creech-Eakman, Joyce A. Guzik, and Robert E. Stencel. *ASP Conference Series* **487***,* Francisco: Astronomical Society of the Pacific, 229-236 (2014).
27. Van Eck, *et al.*, A grid of MARCS model atmospheres for late-type stars. II. S stars and their properties, *Astron. Astrophys*. **601**, A10 (2017).
28. Paladini C., *et al.*, The VLTI/MIDI view on the inner mass loss of evolved stars from the Herschel MESS sample, *Astron. Astrophys.* **600**, A136 (2017).

Extended data

Extended data Figure 1. The PIONIER data. The upper left panel shows in black the PIONIER visibilities, and in blue the Fourier Transform of the SQUEEZE image (first spectral channel). The upper right panel is the same as the previous panel for the closure phase. The lower left panel shows the u-v coverage of the data.

Extended data Figure 2. SQUEEZE images and error images. The first row of images corresponds to the adopted SQUEEZE images; the second row labeled '+STD DEV' corresponds to images one standard deviation above the average image. The third raw of images, labeled '-STD DEV' shows images one standard deviation below the average image.

Extended data Figure 3. Spectral energy distribution. Comparison between the spectral energy distribution (yellow stars) and the best fitting MARCS synthetic spectrum (black line). Note the presence of a moderate infrared excess longwards of 10 µm attributable to circumstellar dust.

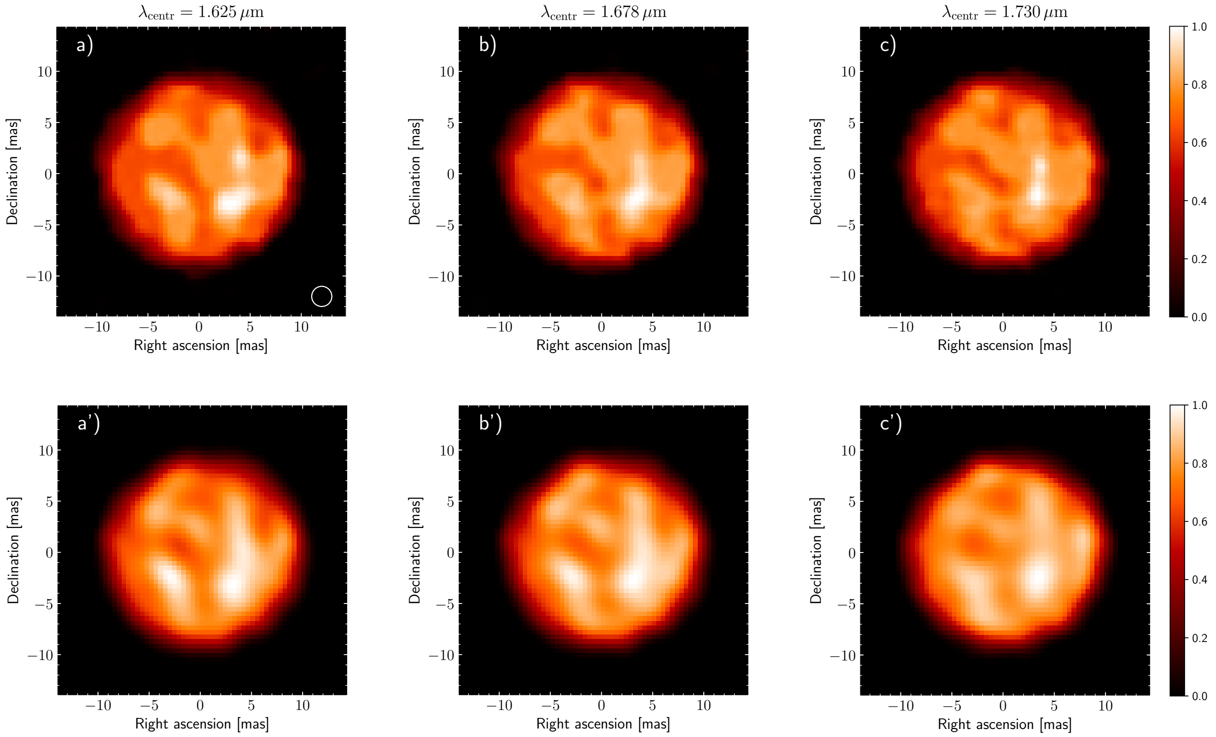
$\lambda_{\rm centr} = 1.625\,\mu$m
$\lambda_{\rm centr} = 1.678\,\mu$m
$\lambda_{\rm centr} = 1.730\,\mu$m
a)
b)
c)
a')
b')
c')
Declination [mas]
Right ascension [mas]
−10
−5
0
5
10
0.0
0.2
0.4
0.6
0.8
1.0

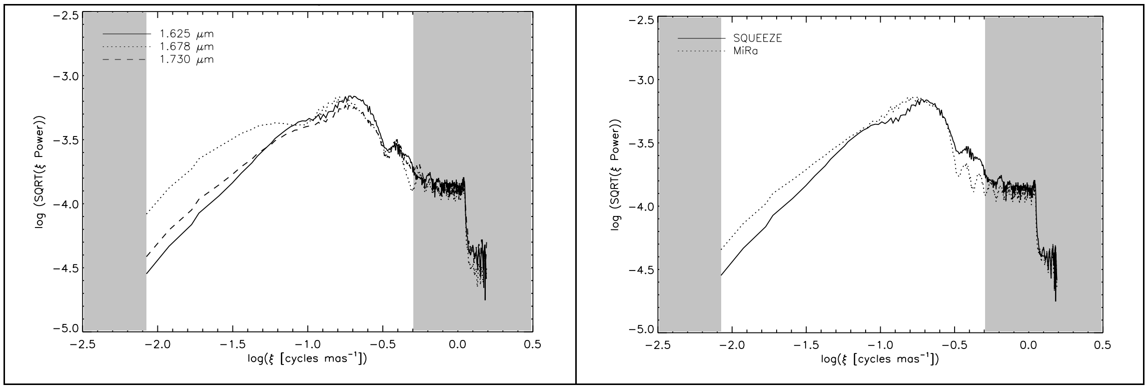
1.625 μm
1.678 μm
1.730 μm
log (SQRT(ξ Power))
log(ξ [cycles mas⁻¹])
−2.5
−3.0
−3.5
−4.0
−4.5
−5.0
−2.5
−2.0
−1.5
−1.0
−0.5
0.0
0.5
SQUEEZE
MiRa

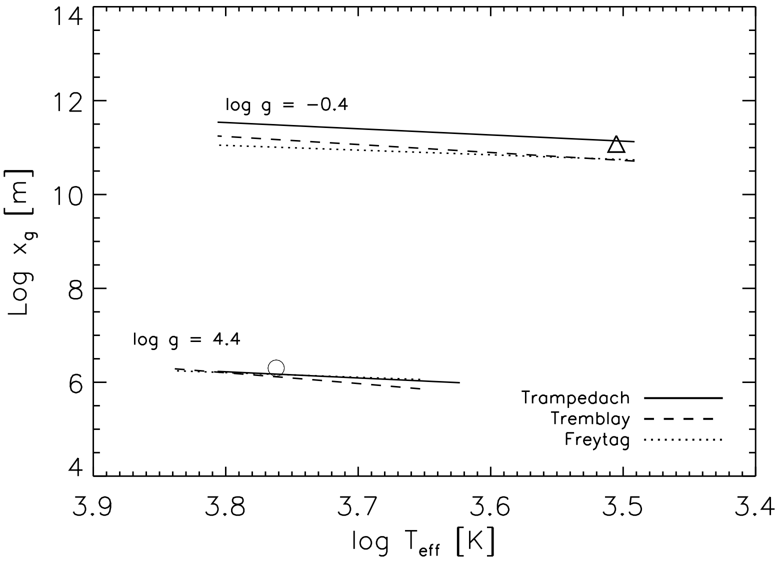
14
12
10
8
6
4
Log x_g [m]
3.9
3.8
3.7
3.6
3.5
3.4
log T_{eff} [K]
log g = −0.4
log g = 4.4
Trampedach
Tremblay
Freytag